

Current Biology

Dopamine and acetylcholine correlations in the nucleus accumbens depend on behavioral task states

Highlights

- Accumbal dopamine and acetylcholine correlations change according to task states
- Dopamine ramps are not correlated with changes in acetylcholine
- Dopamine and acetylcholine dynamics are largely independent
- Correlation pattern indicates that acetylcholine may gate dopamine-based plasticity

Authors

Kauê Machado Costa, Zhewei Zhang, Douglas Deutsch, Yizhou Zhuo, Guochuan Li, Yulong Li, Geoffrey Schoenbaum

Correspondence

kaue.m.costa@gmail.com (K.M.C.), zhewei.zhang@nih.gov (Z.Z.), geoffrey.schoenbaum@nih.gov (G.S.)

In brief

Costa and Zhang et al. show that the correlation between dopamine and acetylcholine in the nucleus accumbens, a region critical for learning and motivation, depends strongly on the behavior an animal is executing. The results indicate that dopamine and acetylcholine act in concert to engage different mechanisms according to task demands.

Report

Dopamine and acetylcholine correlations in the nucleus accumbens depend on behavioral task states

Kauê Machado Costa,^{1,2,9,10,11,*} Zhewei Zhang,^{1,9,*} Douglas Deutsch,¹ Yizhou Zhuo,^{3,4} Guochuan Li,^{3,4} Yulong Li,^{3,4,5,6,7,8} and Geoffrey Schoenbaum^{1,12,*}

¹National Institute on Drug Abuse Intramural Research Program, National Institutes of Health, Baltimore, MD 21224, USA

²Department of Psychology, University of Alabama at Birmingham, Birmingham, AL 35223, USA

³State Key Laboratory of Membrane Biology, School of Life Sciences, Peking University, Beijing 100871, China

⁴PKU-IDG/McGovern Institute for Brain Research, Beijing 100871, China

⁵Peking-Tsinghua Center for Life Sciences, New Cornerstone Science Laboratory, Academy for Advanced Interdisciplinary Studies, Peking University, Beijing 100871, China

⁶Chinese Institute for Brain Research, Beijing 102206, China

⁷Institute of Molecular Physiology, Shenzhen Bay Laboratory, Shenzhen, Guangdong 518055, China

⁸National Biomedical Imaging Center, Peking University, Beijing 100871, China

⁹These authors contributed equally

¹⁰X (formerly Twitter): @kmcostalab

¹¹Bluesky: @kmcostalab.com

¹²Lead contact

*Correspondence: kaue.m.costa@gmail.com (K.M.C.), zhewei.zhang@nih.gov (Z.Z.), geoffrey.schoenbaum@nih.gov (G.S.)

<https://doi.org/10.1016/j.cub.2025.01.064>

SUMMARY

Dopamine release in the nucleus accumbens (NAcc) changes quickly in response to errors in predicting events like reward delivery^{1–3} but also slowly ramps up when animals are moving toward a goal.^{4–10} This ramping has attracted much recent attention, as there is controversy regarding its computational role^{5,7,9,11} and whether they are driven by dopamine neuron firing^{7–9} or local circuit mechanisms.^{5,6} If the latter is true, cholinergic transmission would be a prime candidate mechanism,^{12–14} and acetylcholine and dopamine signals should be positively correlated during behavior, particularly during motivated approach. However, in the dorsal striatum, striatal cholinergic interneurons typically “dip” their activity when reward or associated cues are presented, in opposition to dopamine,^{15–18} and acetylcholine and dopamine release is generally anti-correlated *in vivo*.^{19,20} Furthermore, acetylcholine and dopamine have opposing effects on downstream striatal projection neurons (SPNs),^{21,22} which suggests that cholinergic dips create a permissive window for dopamine to drive plasticity.²³ These studies therefore suggest that dopamine and acetylcholine should be anti-correlated during behavior. We tested between these hypotheses by simultaneously recording accumbal dopamine and acetylcholine signals in rats executing a task involving motivated approach. We found that dopamine ramps were not coincidental with changes in acetylcholine. Instead, acetylcholine was positively, negatively, or uncorrelated with dopamine depending on the task phase. Our results suggest that accumbal dopamine and acetylcholine dynamics are largely independent but may combine to engage different postsynaptic mechanisms depending on task demands.

RESULTS

Experimental procedures and behavioral performance

We transfected 10 male Long-Evans rats with next-generation genetically encoded sensors for dopamine and acetylcholine—rDA3m, a red-shifted dopamine sensor,²⁴ and gACh4h, a novel green acetylcholine sensor. These rats were implanted with optic fiber cannulas in the nucleus accumbens (NAcc) to allow simultaneous multi-color fiber photometry recordings of both dopamine and acetylcholine release dynamics (Figures 1A and 1C).^{1,19,25} We performed post hoc immunohistochemistry and confocal imaging, confirming by visual inspection that there was a high degree of overlap in the expression pattern of gACh4h and rDA3m, especially in cell bodies (Figures 1B and S1). We

quantified the overlap of regions of interest (ROIs) defined by the fluorescent signals associated with each protein and found that the overlap between the two was on average 75.14% ($\pm 6.56\%$ SEM; Figure 1B), indicating that the two sensors were mostly expressed by the same cells. This means that it is unlikely that differences observed in the recorded photometry signals could be attributed to the expression of sensors by widely different cell types.

After at least 4 weeks for recovery and viral expression, rats were water restricted and trained on the behavioral task (Figure 1D). The task was chosen to provide the simplest possible scenario in which dopamine ramps could be expected—a cued, motivated approach behavior. On each trial, the onset of a light cue indicated that rats could perform an entry into a

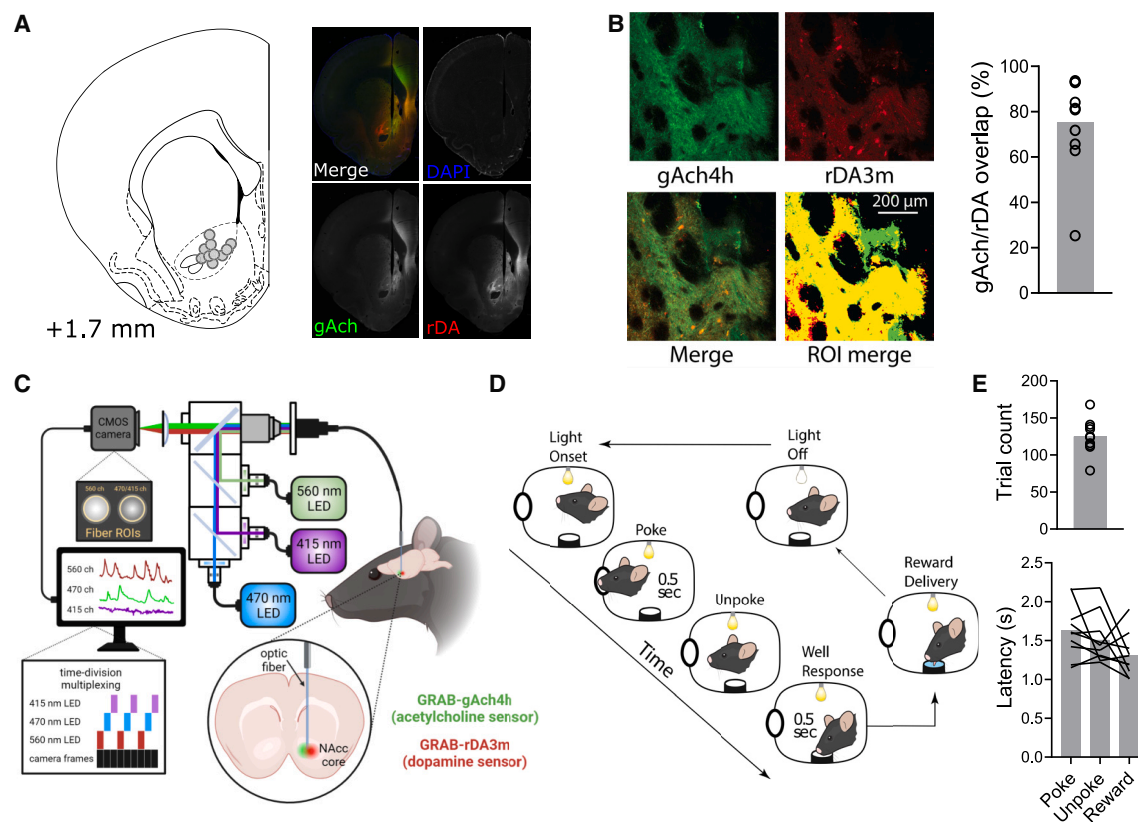


Figure 1. Photometry recordings, histological verification, and behavior

(A) Location of fiber tips in the NAcc for all recorded rats (left; $n = 10$) and representative histological microphotograph (right) with histological detection of both sensors. We would like to highlight that chicken anti-GFP antibodies were the most effective in detecting the gACh4h sensor, out of several alternatives (STAR Methods).

(B) Expression overlap of the two sensors in the NAcc. Photomicrographs are 20 \times confocal images of one exemplar rat (FI02), including images for the green and red channels, the merge of those channels, and the merge of ROIs traced around the expression pattern of each sensor (yellow indicated overlap). The graph represents the quantification of the percentage of area of the ROIs that overlap with each other. Scale bar, 200 μ m.

(C) Cartoon schematic of dual-color fiber photometry recording methods.

(D) Cartoon schematic of the instrumental nose poke task.

(E) Individual and group mean responding of the rats in the behavioral task. Left panel shows the number of trials each rat performed in the 1-h session, and the right panel indicates the time it took for the rats to complete each phase of the task, from light onset to nose poke (poke), from nose poke to unpoke (unpoke), and from unpoke to receiving the reward (reward).

See also Figures S1 and S2.

nose poke port, and after holding this position for 0.5 s, they could perform a second entry into a fluid well, which triggered the delivery of water rewards, also after 0.5 s. Rats learned to perform this task, and analyses reported in this study were on signals collected from one session of each rat ($n = 10$) after they performed >75 trials in a 1-h period for two consecutive sessions. (See Figure S2 for training behavior.) Sessions were limited to 1 h to avoid excessive photobleaching, and the rats performed an average of 125 trials in the analyzed recording session and completed trials in a relatively similar time frame (Figure 1E).

The analyses reported here were conducted mainly on signals that were only detrended (to remove photobleaching artifacts), median filtered (to remove high-frequency artifacts), and Z scored (to allow for better comparisons between sessions and subjects). We did record fluorescence elicited by 415 nm excitation, but the use of this “isosbestic” control has recently been

called into question.²⁶ We found that referencing our signals to the 415 channel did not affect the interpretation of the signal dynamics (Figure S3), but we chose to continue with the most conservative approach.

Dopamine and acetylcholine correlations vary according to task phase

Analysis of the dopamine and acetylcholine signals clearly demonstrated that they were not uniformly correlated across the different phases of the approach task (Figure 2). When we aligned the two signals to the nose poke, we observed clear dopamine ramps, gradual increases in dopamine signal as the rats approached the goal, replicating several recent findings.^{4–6} These ramps were significantly different from a shuffled control signal, crossing the shuffled threshold well before the rats actually executed the nose poke (indicated by the colored bars on top of the signals in Figure 2), and their time course matched the time

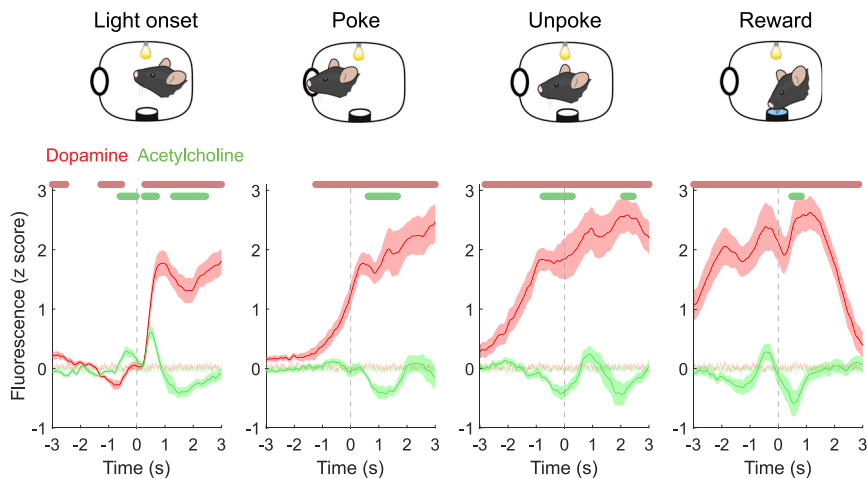


Figure 2. NAcc dopamine and acetylcholine dynamics during the instrumental task

Graphical representation of the task event to which each graph below is aligned (dashed gray line) and dopamine (red) and acetylcholine (green) signals aligned to the task events. Note that there is an increase in both signals immediately after light onset, a progressive dopamine ramp with no significant change in cholinergic signal prior to the nose poke, a phasic increase in dopamine right after the poke, a dip in acetylcholine centered around the unpoke and followed by an increase in dopamine, and an increase in dopamine and dip in acetylcholine immediately after the reward delivery. The number of trials for each animal is the same as reported in [Figures 1D](#) and [S2](#). Data are represented as mean \pm 95% CI. Light green and light red shades in the background are the SEM of the shuffled baseline control. Colored bars above graphs indicate significant difference from shuffled control using a permutation test.²⁷ See also [Figures S3](#) and [S4](#).

course of behavioral responding during this phase ([Figure 1D](#)). However, acetylcholine signals in the same period did not change during this phase, remaining statistically similar to the shuffled control prior to the poke.

Furthermore, a comparison of the slopes of the dopamine and acetylcholine signals during the 1-s period immediately preceding the poke demonstrated that acetylcholine signals do not show a consistent positive slope as dopamine signals ramp up and that the slopes of the two signals are not correlated ([Figure S4](#)). Moreover, in a subset of rats ($n = 6$) we compared dopamine and acetylcholine dynamics preceding nose pokes performed during rewarded trials and during the intertrial intervals (ITIs), where the rats could not obtain rewards. Dopamine ramps only occurred during rewarded trials and were absent in the ITIs, suggesting that the ramps are driven by the expectation of reward, not the poke movement itself ([Figure S6A](#)). In the same period, acetylcholine signal slopes were not different between trials and ITIs ([Figures S6A](#) and [S6B](#)), confirming that neither the motivated approach nor the poke movement itself is related to significant changes in cholinergic dynamics. This compounded evidence goes against the predictions that the dopamine ramps are caused by local cholinergic depolarization of dopamine axons or that accumbal acetylcholine signals translate motivation into dopamine release.

However, the relationship between dopamine and acetylcholine signals was different during other task phases. When we aligned signals to the unpoke, which was the action immediately prior to reward seeking, we observed a phasic increase in dopamine and a coincidental decrease in acetylcholine. The same was observed when we aligned the signals to reward port entry, with dopamine rises and acetylcholine dips occurring around the time of reward delivery. This indicated that whenever the task involved a rewarded action, or reward itself, dopamine and acetylcholine signals became anti-correlated, with a characteristic burst in dopamine and dip in acetylcholine. Finally, we also found periods when the two signals were correlated. For example, when the light was turned on, indicating the start of the trial, both dopamine and acetylcholine signals showed sharp increases (although these were also followed by a dip).

Dopamine and acetylcholine cross-correlations differ according to task phase

We next asked if the cross-correlations within and between the two signals were also different depending on task phase ([Figure 3A](#)). This was done to rule out any potential lagged correlation that could indicate a causal relationship between the signals. We performed cross-correlation analysis on the two signals during the baseline (right before trial start), ramping (before the nose poke), and around the light on, nose poke, unpoke, and reward port entry timestamps, with lags computed relative to the dopamine signal. We found that during baseline, light onset, ramping, and nose poke, states not directly related to reward, the two signals had significant positive cross-correlations at a lag of between 100 and 150 ms relative to dopamine ([Figures 3B](#) and [3C](#)), with the largest positive correlation occurring during the light onset state (see [Tables S1–S4](#) for post hoc multiple-comparison tests). However, during the unpoke and the reward phase, which were more proximal to reward, there were essentially no positive correlation peaks, and the lags of the maximal correlation coefficients are in the measurement boundaries of 1 and -1 s. Conversely, there were also significant differences in the peak anti-correlation (most negative coefficient) for each phase ([Figure 3D](#)), with values during the light onset being the least negative. The clearest difference was in the lag of the anti-correlation peak, which was most negative during the ramp phase and progressively approached zero toward the reward phase ([Figure 3D](#)). We also computed the autocorrelation for each signal in the same time windows ([Figure S5](#)). These analyses further confirm that the cross-channel dynamics of dopamine and acetylcholine photometry differ depending on the task state.

Dopamine and acetylcholine signal dynamics are largely independent

We further tested if there was any signature in the dopamine and acetylcholine signals that could indicate a causal relationship between the two neuromodulator dynamics. For this, we removed the variance in each signal that could be explained by the variance in the other signal. In brief, we fitted a kernel function to the dopamine signal, took the parameters of that fit and

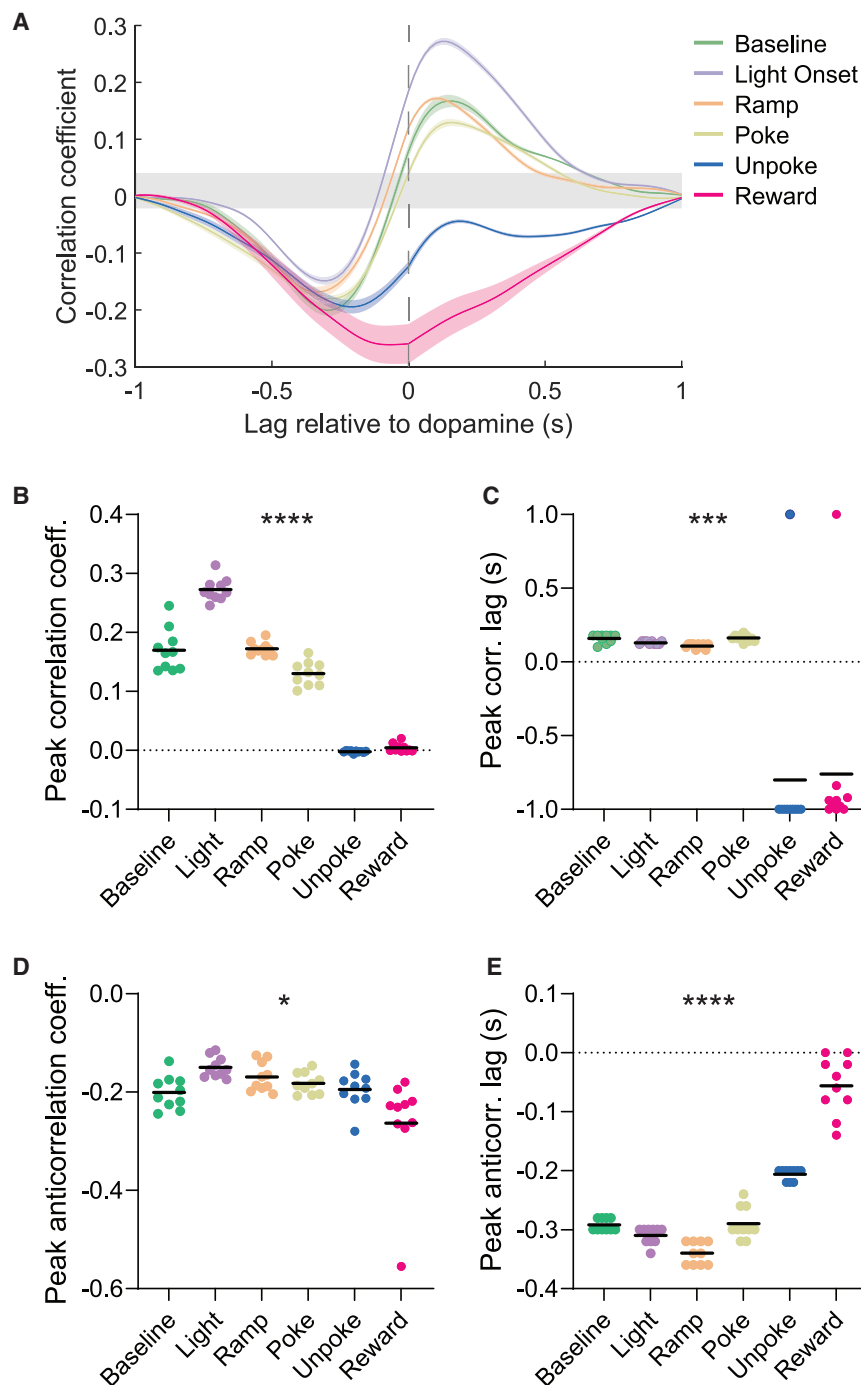


Figure 3. Cross-correlations between dopamine and acetylcholine signals vary according to task phase alignment

(A) Cross-correlation between dopamine and acetylcholine signals in the NAcc during different periods of the task ($n = 10$ rats). Gray patch is the 95% confidence interval of a shuffled control, and colored shared are SEMs.

(B) Correlation coefficient (Pearson's r) at the point of maximal correlation between the signals.

(C) Lag of the point of maximal correlation between the signals.

(D) Correlation coefficient at the point of minimal correlation (peak anti-correlation) between the signals.

(E) Lag of the point of minimal correlation between the signals. Post hoc test results are shown in Tables S1–S4. Lines in graphs represent the mean. * $p < 0.05$, *** $p < 0.001$, **** $p < 0.0001$.

See also Figure S5.

dopamine ramps preceding the nose poke, dopamine rises and acetylcholine dips during the reward-related epochs, and dopamine and acetylcholine rises to the light on. This preservation suggests that, while dopamine and acetylcholine signals may be correlated during these events, their variance is largely independent, which indicates it is unlikely that one signal directly causes changes to the other. This is in line with recent work in the dorsal striatum that indicated that dopamine and acetylcholine signals are autonomously controlled by extra-striatal afferents.¹⁹

To further test this, we applied generalized linear model (GLM) regressions to measure event-related effects on the photometry signal dynamics, using the task events as kernels.^{28,29} We found that dopamine and acetylcholine regression coefficients were significantly different for every task event, including the approach period related to dopamine ramps (Figure 4C). This confirmed that event-related effects on signal variance were different for dopamine and acetylcholine. This also confirmed the absence

of dopamine ramping during ITIs and of significant differences in event-related cholinergic responses (Figures S6C and S6D). Taken together, these different regression methods demonstrate that accumbal dopamine and acetylcholine dynamics, including responses to task events, are statistically independent.

applied them to acetylcholine signal, subtracted the resulting fit from the original acetylcholine signal, and repeated the same process with acetylcholine being the first fit and dopamine the second. The end results were dopamine and acetylcholine signals that were free of the variance explained by the dynamics of the other simultaneously recorded signal, and in which their dynamics could be compared in a scale-invariant manner (Figures 4A and 4B).

We found that after this processing, the main patterns we had observed in the raw signals were all preserved. This included the

DISCUSSION

We simultaneously recorded dopamine and acetylcholine signals in the NAcc while rats performed an instrumental task that

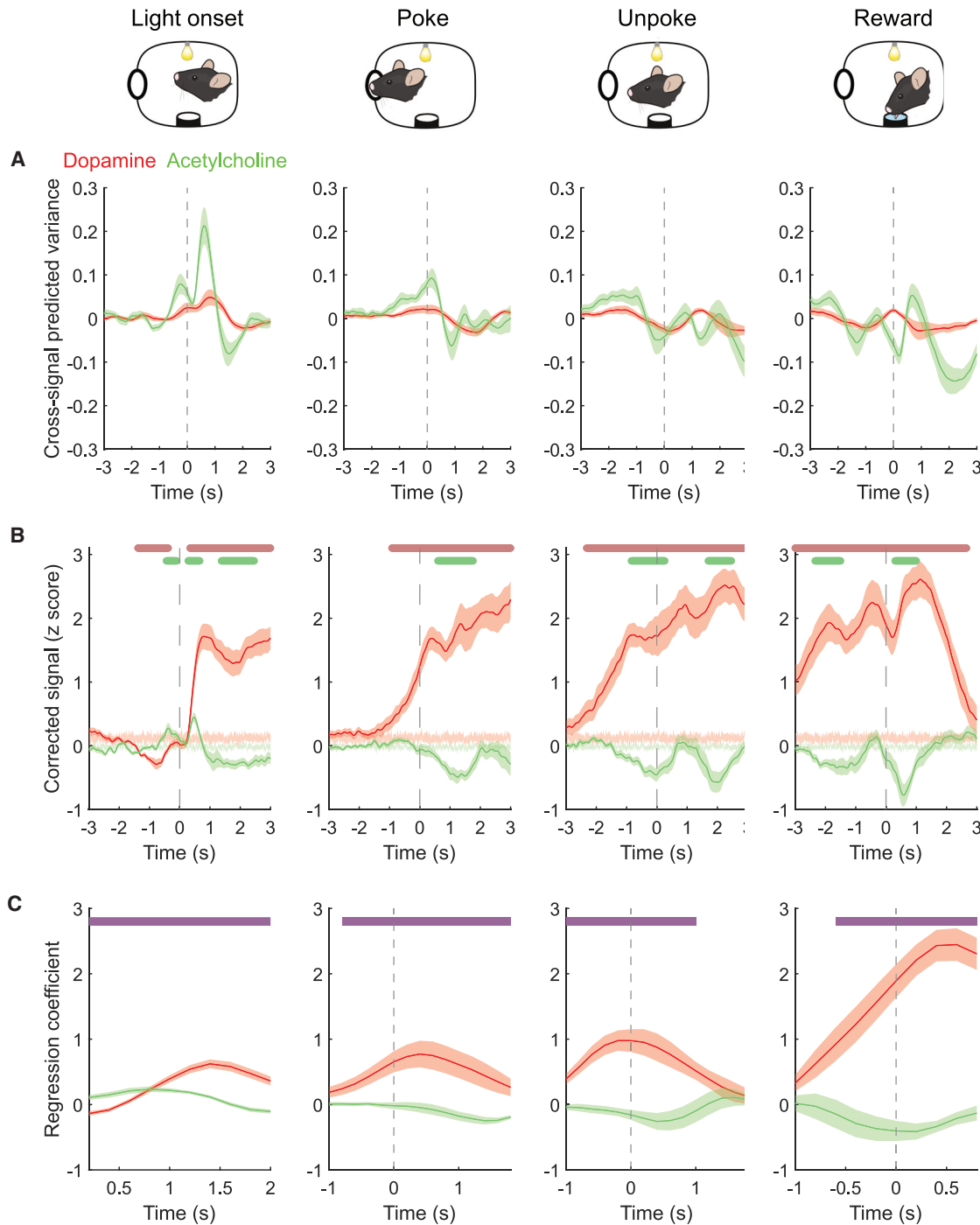


Figure 4. Accumbal dopamine and acetylcholine dynamics are largely independent

(A) Average traces of the acetylcholine signal variance explained by dopamine dynamics (green) and the dopamine signal variance explained by acetylcholine dynamics (red) for each task phase.

(B) Dopamine (red) and acetylcholine (green) signals where the variance explained by the dynamics of the alternative signal have been removed. Note that the major patterns of activity, including anticipatory dopamine ramps and cholinergic dips during reward and rewarded action, are largely similar. Data are represented as mean \pm SEM. Light green and light red shades in the background are the SEM of the shuffled baseline control. Colored bars above graphs indicate significant difference from shuffled control using a permutation test.²⁷

(C) Purple bars above the plots indicate significant difference ($p < 0.05$) between dopamine and acetylcholine regression coefficients using t tests for each 0.2 s bin.

See also Figure S6.

involved motivated approach. We found that dopamine and acetylcholine signal correlations vary widely depending on the task state and the associated behavior. Essentially, dopamine and acetylcholine were positively correlated in response to the light cue that started the trial, uncorrelated during anticipatory ramps, and anti-correlated during task phases that involved reward or a directly rewarded action.

Critically, the lack of correlation between dopamine ramps and changes in acetylcholine during motivated approach demonstrates that this form of dopamine signaling is likely not driven by local acetylcholine release. Our findings contradict previous work, which suggested that cholinergic interneurons generate dopamine ramps.⁶ However, that study used fiber photometry to record calcium signals, which can be uncoupled from somatic firing and neurotransmitter release.³⁰ Furthermore, the causal optogenetic evidence presented in that paper has been argued to be an artifact of direct optical stimulation of the calcium sensor.³¹ Our study, which employed a more direct measure of dopamine and acetylcholine signaling in NAcc during behavior, failed to replicate this relationship.

That said, there are methodological limits to consider when interpreting our findings. Photometry recordings sample a relatively large area of neural tissue, with no cell-type specificity, so there is still the possibility that there are variations in dopamine-acetylcholine interactions at the cellular and subcellular levels that were not captured with our methods. Nevertheless, our findings are well in line with most of the previous literature, and signals recorded at the resolution level of photometry are typically correlated with and causally linked to behavioral performance.^{2,7,26}

Our findings are also in line with previous electrophysiological and photometry studies of cholinergic transmission in the dorsal striatum. Cholinergic interneurons in the dorsal striatum tend to pause in response to reward and reward-predicting cues while dopamine neurons tend to burst in the same conditions,¹⁵ and dopamine and acetylcholine release in the dorsal striatum is anti-correlated during reward,^{19,20} both patterns that fit with our dual photometry results in the NAcc. Additionally, individual striatal cholinergic interneurons have also been found to burst, or burst and then dip, in response to cued events, similarly to what we observed in response to the light onset.^{15–18} This suggests that the general local circuit structure governing dopamine and acetylcholine release in the NAcc is somewhat similar to what has been described for the dorsal striatum. Recent findings in the NAcc with non-simultaneous dopamine and acetylcholine recordings and a Pavlovian task design also support this conclusion and are in line with our results.³²

Some authors propose that accumbal dopamine ramps do not reflect prediction errors but instead signal the absolute value expectation or motivation associated with the goal.⁵ Alternatively, others suggest that the ramps can be explained by slight modifications to classical temporal difference learning algorithms^{7,33} or that they are a correlate of the use of cognitive maps.⁹ The idea that these ramps have a behavioral role that is distinct from reward prediction error signaling is linked to the idea that these ramps also may be generated by different mechanisms.^{5,6} We found that acetylcholine changes are not a prerequisite for dopamine ramping, which suggests that dopamine ramps likely share the same mechanisms, at least presynaptically, as other dopamine signaling events, like classical reward

prediction errors. However, it is conspicuous that we observed an anti-correlation between dopamine and acetylcholine in the precise epochs that dopamine should be signaling reward prediction errors and, presumably, driving reward-related learning. Specifically, cholinergic dips and dopamine increases coincide with events that are intrinsically rewarding or have been directly associated with reward. This indicates that, even if the ramps and classical prediction error signals are generated by the same presynaptic mechanisms, they may engage different postsynaptic targets.

The anti-correlation pattern fits well with the finding that dopamine and acetylcholine exert opposing effects on each classical striatal projection neuron (SPN) pathway. In the direct pathway, dopamine acts on D1 receptors while acetylcholine acts on M4 receptors, respectively, boosting and decreasing synaptic plasticity.²¹ In the indirect pathway, dopamine acts on D2 receptors and acetylcholine acts on M1 receptors, which also exert opposing effects on plasticity in these SPNs.²² It has been proposed that this oppositional relationship creates a tripartite condition for synaptic plasticity to occur in each pathway, and learning occurs primarily when there is a coincidental dopamine burst, acetylcholine dip, and postsynaptic depolarization.²³ That said, the real situation is almost certainly more complex, as both modulators also act on different interneurons and on dopamine axons themselves,^{13,14,34,35} and there is compounding evidence that both direct and indirect SPNs are co-active during learning and decision-making.^{28,36–39} The mechanistic model described previously is intended as an initial heuristic for investigating dopamine and acetylcholine interactions in subsequent studies.

Within this framework, the fact that dopamine and acetylcholine are not anti-correlated during motivated approach and salient cue exposure is remarkable. This suggests that during these epochs, the combined postsynaptic effect of both neuromodulators may be quite different. It also indicates that dopamine ramps and cue responses are indeed mechanistically different from classical reward prediction error responses, at least in how they modulate downstream targets. While all these dopamine responses can be conceptualized as prediction errors, reward-based or otherwise,^{1,7} they clearly drive different behaviors, and therefore it would make sense that they engage different postsynaptic mechanisms. Regarding specifically the dip in acetylcholine during dopamine reward prediction error signaling, it could be that the dips reflect the associative salience of the actions and reward and create a critical window where dopamine can drive associative learning-related plasticity.^{40,41} This possibility should be explored in future work.

The correlated responses to the light cue are harder to interpret within the confines of our task. This cue is related to reward availability and indicates that the rat can initiate an action; therefore, the cholinergic responses could be related both to an action initiation and value. However, it is worth noting that in this task the light onset is the only highly salient cue that is outside of the rat's control, and thus the dopaminergic and cholinergic responses to this event may be dominated by physical salience or a sensory prediction error.^{1,42–44} Future work with more complex tasks will be needed to disambiguate the nature of these responses.

Our findings indicate that the correlation between dopamine and acetylcholine release in the NAcc is heavily dependent on the precise timing and type of behavioral processes. Dopamine

increases in response to most events in this task, but acetylcholine dips during events directly related to reward and peaks during salient trial-setting cues. Importantly, anticipatory dopamine ramps are not coincidental with changes in cholinergic signals. This pattern of results suggests that different behavior-related dopamine signals may induce specific postsynaptic effects in NAcc neurons depending on their interaction with acetylcholine dynamics.

RESOURCE AVAILABILITY

Lead contact

Further information and requests for resources and reagents should be directed to and will be fulfilled by the lead contact, Geoffrey Schoenbaum (geoffrey.schoenbaum@nih.gov).

Materials availability

This study did not generate new, unique reagents.

Data and code availability

- Data and code used in this paper are publicly available at Zenodo: <https://doi.org/10.5281/zenodo.14729705>.
- Any additional information required to reanalyze the data reported in this paper is available from the [lead contact](#) upon request.

ACKNOWLEDGMENTS

This work was supported by the Intramural Research Program at the National Institute on Drug Abuse (ZIA DA000587 to G.S. and R00 DA055641 to K.M.C.) and by the NIH BRAIN Initiative (NINDS U01NS120824 to Y.L.). We thank Nicolas Tritsch for his constructive comments on the study. We thank Shiliang Steven Zhang and the NIDA IRP Histology and Imaging Core for assistance with antibody testing and histological processing. The opinions expressed in this article are the authors' own and do not reflect the view of the NIH/DHHS.

AUTHOR CONTRIBUTIONS

Conceptualization, K.M.C., Z.Z., and G.S.; data curation, K.M.C. and Z.Z.; formal analysis, K.M.C. and Z.Z.; funding acquisition, Y.L. and G.S.; investigation, K.M.C., Z.Z., and D.D.; methodology, K.M.C., Z.Z., Y.Z., G.L., and Y.L.; project administration, G.S.; software, K.M.C. and Z.Z.; resources, Y.Z., G.L., and Y.L.; supervision, G.S.; validation, K.M.C., Z.Z., Y.Z., G.L., and Y.L.; visualization, K.M.C. and Z.Z.; writing – original draft, K.M.C.; writing – review and editing, K.M.C., Z.Z., and G.S.

DECLARATION OF INTERESTS

The authors declare no competing interests.

STAR★METHODS

Detailed methods are provided in the online version of this paper and include the following:

- [KEY RESOURCES TABLE](#)
- [EXPERIMENTAL MODEL AND SUBJECT DETAILS](#)
- [METHOD DETAILS](#)
 - Surgical procedures
 - Dual color fiber photometry
 - Histological procedures
- [QUANTIFICATION AND STATISTICAL ANALYSIS](#)
 - Signal analysis
 - Generalized linear model analysis
 - Behavioral apparatus and instrumental nose poke task
 - Expression overlap analysis
 - Statistical analysis

SUPPLEMENTAL INFORMATION

Supplemental information can be found online at <https://doi.org/10.1016/j.cub.2025.01.064>.

Received: May 28, 2024

Revised: December 13, 2024

Accepted: January 28, 2025

Published: March 3, 2025

REFERENCES

1. Costa, K.M., Raheja, N., Mirani, J., Sercander, C., and Schoenbaum, G. (2023). Striatal dopamine release reflects a domain-general prediction error. Preprint at bioRxiv. <https://doi.org/10.1101/2023.08.19.553959>.
2. Menegas, W., Babayan, B.M., Uchida, N., and Watabe-Uchida, M. (2017). Opposite initialization to novel cues in dopamine signaling in ventral and posterior striatum in mice. *eLife* 6, e21886. <https://doi.org/10.7554/eLife.21886>.
3. Costa, K.M., and Schoenbaum, G. (2022). Dopamine. *Curr. Biol.* 32, R817–R824. <https://doi.org/10.1016/J.CUB.2022.06.060>.
4. Howe, M.W., Tierney, P.L., Sandberg, S.G., Phillips, P.E.M., and Graybiel, A.M. (2013). Prolonged dopamine signalling in striatum signals proximity and value of distant rewards. *Nature* 500, 575–579. <https://doi.org/10.1038/nature12475>.
5. Mohebi, A., Pettibone, J.R., Hamid, A.A., Wong, J.T., Vinson, L.T., Patriarchi, T., Tian, L., Kennedy, R.T., and Berke, J.D. (2019). Dissociable dopamine dynamics for learning and motivation. *Nature* 570, 65–70. <https://doi.org/10.1038/s41586-019-1235-y>.
6. Mohebi, A., Collins, V.L., and Berke, J.D. (2023). Accumbens cholinergic interneurons dynamically promote dopamine release and enable motivation. *eLife* 12, e85011. <https://doi.org/10.7554/eLife.85011>.
7. Kim, H.R., Malik, A.N., Mikhael, J.G., Bech, P., Tsutsui-Kimura, I., Sun, F., Zhang, Y., Li, Y., Watabe-Uchida, M., Gershman, S.J., et al. (2020). A unified framework for dopamine signals across timescales. *Cell* 183, 1600–1616.e25. <https://doi.org/10.1016/j.cell.2020.11.013>.
8. de Jong, J.W., Liang, Y., Verharen, J.P.H., Fraser, K.M., and Lammel, S. (2024). State and rate-of-change encoding in parallel mesoaccumbal dopamine pathways. *Nat. Neurosci.* 27, 309–318. <https://doi.org/10.1038/s41593-023-01547-6>.
9. Guru, A., Seo, C., Post, R.J., Kullakanda, D.S., Schaffer, J.A., and Warden, M.R. (2020). Ramping activity in midbrain dopamine neurons signifies the use of a cognitive map. Preprint at bioRxiv. <https://doi.org/10.1101/2020.05.21.108886>.
10. Chow, J.J., Pitts, K.M., Schoenbaum, A., Costa, K.M., Schoenbaum, G., and Shaham, Y. (2024). Different effects of peer sex on operant responding for social interaction and striatal dopamine activity. *J. Neurosci.* 44, e1887232024. <https://doi.org/10.1523/JNEUROSCI.1887-23.2024>.
11. Gershman, S.J. (2014). Dopamine ramps are a consequence of reward prediction errors. *Neural Comput.* 26, 467–471. https://doi.org/10.1162/NECO_a_00559.
12. Rice, M.E., and Cragg, S.J. (2004). Nicotine amplifies reward-related dopamine signals in striatum. *Nat. Neurosci.* 7, 583–584. <https://doi.org/10.1038/nn1244>.
13. Kramer, P.F., Brill-Weil, S.G., Cummins, A.C., Zhang, R., Camacho-Hernandez, G.A., Newman, A.H., Eldridge, M.A.G., Averbeck, B.B., and Khaliq, Z.M. (2022). Synaptic-like axo-axonal transmission from striatal cholinergic interneurons onto dopaminergic fibers. *Neuron* 110, 2949–2960.e4. <https://doi.org/10.1016/j.neuron.2022.07.011>.
14. Zhang, Y.-F., Luan, P., Qiao, Q., He, Y., Zatzka-Haas, P., Zhang, G., Lin, M.Z., Lak, A., Jing, M., Mann, E.O., et al. (2024). An axonal brake on striatal dopamine output by cholinergic interneurons. Preprint at bioRxiv. <https://doi.org/10.1101/2024.02.17.580796>.

15. Morris, G., Arkadir, D., Nevet, A., Vaadia, E., and Bergman, H. (2004). Coincident but distinct messages of midbrain dopamine and striatal tonically active neurons. *Neuron* 43, 133–143. <https://doi.org/10.1016/j.neuron.2004.06.012>.
16. Apicella, P., Scarnati, E., and Schultz, W. (1991). Tonically discharging neurons of monkey striatum respond to preparatory and rewarding stimuli. *Exp. Brain Res.* 84, 672–675. <https://doi.org/10.1007/BF00230981>.
17. Deffains, M., and Bergman, H. (2015). Striatal cholinergic interneurons and cortico-striatal synaptic plasticity in health and disease. *Mov. Disord.* 30, 1014–1025. <https://doi.org/10.1002/mds.26300>.
18. Aosaki, T., Kimura, M., and Graybiel, A.M. (1995). Temporal and spatial characteristics of tonically active neurons of the primate's striatum. *J. Neurophysiol.* 73, 1234–1252. <https://doi.org/10.1152/jn.1995.73.3.1234>.
19. Krok, A.C., Maltese, M., Mistry, P., Miao, X., Li, Y., and Tritsch, N.X. (2023). Intrinsic dopamine and acetylcholine dynamics in the striatum of mice. *Nature* 621, 543–549. <https://doi.org/10.1038/s41586-023-05995-9>.
20. Chantranupong, L., Beron, C.C., Zimmer, J.A., Wen, M.J., Wang, W., and Sabatini, B.L. (2023). Dopamine and glutamate regulate striatal acetylcholine in decision-making. *Nature* 621, 577–585. <https://doi.org/10.1038/s41586-023-06492-9>.
21. Shen, W., Plotkin, J.L., Francardo, V., Ko, W.K.D., Xie, Z., Li, Q., Fieblinger, T., Wess, J., Neubig, R.R., Lindsley, C.W., et al. (2015). M4 muscarinic receptor signaling ameliorates striatal plasticity deficits in models of L-dopa-induced dyskinesia. *Neuron* 88, 762–773. <https://doi.org/10.1016/j.neuron.2015.10.039>.
22. Shen, W., Tian, X., Day, M., Ulrich, S., Tkatch, T., Nathanson, N.M., and Surmeier, D.J. (2007). Cholinergic modulation of Kir2 channels selectively elevates dendritic excitability in striatopallidal neurons. *Nat. Neurosci.* 10, 1458–1466. <https://doi.org/10.1038/nn1972>.
23. Reynolds, J.N.J., Avvisati, R., Dodson, P.D., Fisher, S.D., Oswald, M.J., Wickens, J.R., and Zhang, Y.-F. (2022). Coincidence of cholinergic pauses, dopaminergic activation and depolarisation of spiny projection neurons drives synaptic plasticity in the striatum. *Nat. Commun.* 13, 1296. <https://doi.org/10.1038/s41467-022-28950-0>.
24. Zhuo, Y., Luo, B., Yi, X., Dong, H., Miao, X., Wan, J., Williams, J.T., Campbell, M.G., Cai, R., Qian, T., et al. (2024). Improved green and red GRAB sensors for monitoring dopaminergic activity in vivo. *Nat. Methods* 21, 680–691. <https://doi.org/10.1038/s41592-023-02100-w>.
25. Martianova, E., Aronson, S., and Proulx, C.D. (2019). Multi-fiber photometry to record neural activity in freely-moving animals. *J. Vis. Exp.* <https://doi.org/10.3791/60278>.
26. Simpson, E.H., Akam, T., Patriarichi, T., Blanco-Pozo, M., Burgeno, L.M., Mohebi, A., Cragg, S.J., and Walton, M.E. (2024). Lights, fiber, action! A primer on *in vivo* fiber photometry. *Neuron* 112, 718–739. <https://doi.org/10.1016/j.neuron.2023.11.016>.
27. Jean-Richard-dit-Bressel, P., Clifford, C.W.G., and McNally, G.P. (2020). Analyzing event-related transients: confidence intervals, permutation tests, and consecutive thresholds. *Front. Mol. Neurosci.* 13, 14. <https://doi.org/10.3389/fnmol.2020.00014>.
28. Desevye, C., Domingues, A.V., Carvalho, T.T.A., Armada, G., Correia, R., Vieitas-Gaspar, N., Wezik, M., Pinto, L., Sousa, N., Coimbra, B., et al. (2024). Nucleus accumbens neurons dynamically respond to appetitive and aversive associative learning. *J. Neurochem.* 168, 312–327. <https://doi.org/10.1111/jnc.16063>.
29. Parker, N.F., Cameron, C.M., Taliaferro, J.P., Lee, J., Choi, J.Y., Davidson, T.J., Daw, N.D., and Witten, I.B. (2016). Reward and choice encoding in terminals of midbrain dopamine neurons depends on striatal target. *Nat. Neurosci.* 19, 845–854. <https://doi.org/10.1038/nn.4287>.
30. Legaria, A.A., Matikainen-Ankney, B.A., Yang, B., Ahanonu, B., Licholai, J.A., Parker, J.G., and Kravitz, A.V. (2022). Fiber photometry in striatum reflects primarily nonsomatic changes in calcium. *Nat. Neurosci.* 25, 1124–1128. <https://doi.org/10.1038/s41593-022-01152-z>.
31. Taniguchi, J., Melani, R., Chantranupong, L., Wen, M.J., Mohebi, A., Berke, J., Sabatini, B., and Tritsch, N. (2024). Comment on ‘accumbens cholinergic interneurons dynamically promote dopamine release and enable motivation. Preprint at bioRxiv. <https://doi.org/10.1101/2023.12.27.573485>.
32. Skirzewski, M., Princz-Lebel, O., German-Castelan, L., Crooks, A.M., Kim, G.K., Tarnow, S.H., Reichelt, A., Memar, S., Palmer, D., Li, Y., et al. (2022). Continuous cholinergic-dopaminergic updating in the nucleus accumbens underlies approaches to reward-predicting cues. *Nat. Commun.* 13, 7924. <https://doi.org/10.1038/s41467-022-35601-x>.
33. Farrell, K., Lak, A., and Saleem, A.B. (2022). Midbrain dopamine neurons signal phasic and ramping reward prediction error during goal-directed navigation. *Cell Rep.* 41, 111470. <https://doi.org/10.1016/j.celrep.2022.111470>.
34. Clarke, R., and Adermark, L. (2015). Dopaminergic regulation of striatal interneurons in reward and addiction: focus on alcohol. *Neural Plast.* 2015, 814567. <https://doi.org/10.1155/2015/814567>.
35. Ford, C.P. (2014). The role of D2-autoreceptors in regulating dopamine neuron activity and transmission. *Neuroscience* 282, 13–22. <https://doi.org/10.1016/j.neuroscience.2014.01.025>.
36. Cui, G., Jun, S.B., Jin, X., Pham, M.D., Vogel, S.S., Lovinger, D.M., and Costa, R.M. (2013). Concurrent activation of striatal direct and indirect pathways during action initiation. *Nature* 494, 238–242. <https://doi.org/10.1038/nature11846>.
37. Soares-Cunha, C., Coimbra, B., Sousa, N., and Rodrigues, A.J. (2016). Reappraising striatal D1- and D2-neurons in reward and aversion. *Neurosci. Biobehav. Rev.* 68, 370–386. <https://doi.org/10.1016/j.neurobiorev.2016.05.021>.
38. Zachry, J.E., Kuttlu, M.G., Yoon, H.J., Leonard, M.Z., Chevée, M., Patel, D.D., Gaidici, A., Kondev, V., Thibeault, K.C., Bethi, R., et al. (2024). D1 and D2 medium spiny neurons in the nucleus accumbens core have distinct and valence-independent roles in learning. *Neuron* 112, 835–849.e7. <https://doi.org/10.1016/j.neuron.2023.11.023>.
39. Domingues, A.V., Carvalho, T.T.A., Martins, G.J., Correia, R., Coimbra, B., Bastos-Gonçalves, R., Wezik, M., Gaspar, R., Pinto, L., Sousa, N., et al. (2025). Dynamic representation of appetitive and aversive stimuli in nucleus accumbens shell D1- and D2-medium spiny neurons. *Nat. Commun.* 16, 59. <https://doi.org/10.1038/s41467-024-55269-9>.
40. Brown, M.T.C., Tan, K.R., O'Connor, E.C., Nikonenko, I., Muller, D., and Lüscher, C. (2012). Ventral tegmental area GABA projections pause accumbal cholinergic interneurons to enhance associative learning. *Nature* 492, 452–456. <https://doi.org/10.1038/nature11657>.
41. Cragg, S.J. (2006). Meaningful silences: how dopamine listens to the ACh pause. *Trends Neurosci.* 29, 125–131. <https://doi.org/10.1016/j.tins.2006.01.003>.
42. Bromberg-Martin, E.S., Matsumoto, M., and Hikosaka, O. (2010). Dopamine in motivational control: rewarding, aversive, and alerting. *Neuron* 68, 815–834. <https://doi.org/10.1016/j.neuron.2010.11.022>.
43. Shapovalova, K.B. (1999). Activation of the cholinergic system of the striatum improves attention to conditioned reflex stimuli. *Neurosci. Behav. Physiol.* 29, 493–503. <https://doi.org/10.1007/BF02461141>.
44. Ding, J.B., Guzman, J.N., Peterson, J.D., Goldberg, J.A., and Surmeier, D.J. (2010). Thalamic gating of corticostriatal signaling by cholinergic interneurons. *Neuron* 67, 294–307. <https://doi.org/10.1016/j.neuron.2010.06.017>.
45. Schindelin, J., Arganda-Carreras, I., Frise, E., Kaynig, V., Longair, M., Pietzsch, T., Preibisch, S., Rueden, C., Saalfeld, S., Schmid, B., et al. (2012). Fiji: an open-source platform for biological-image analysis. *Nat. Methods* 9, 676–682. <https://doi.org/10.1038/nmeth.2019>.
46. Lopes, G., Bonacchi, N., Frazão, J., Neto, J.P., Atallah, B.V., Soares, S., Moreira, L., Matias, S., Itskov, P.M., Correia, P.A., et al. (2015). Bonsai: an event-based framework for processing and controlling data streams. *Front. Neuroinform.* 9, 7. <https://doi.org/10.3389/FNINF.2015.00007>.

STAR★METHODS

KEY RESOURCES TABLE

REAGENT or RESOURCE	SOURCE	IDENTIFIER
Antibodies		
Chicken anti-GFP	Abcam USA	RRID:AB_300798
Rabbit anti-DsRED	Takara Bio USA	RRID:AB_10013483
Donkey anti-chicken Alexa Fluor 488	Abcam USA	RRID:AB_2340375
Donkey anti-rabbit Alexa Fluor 594	Abcam USA	RRID:AB_2340621
Bacterial and virus strains		
AAV2/9-hsyn-rDA3m	Zhuo et al. ²⁴	BrainVTA: PT-4746
AAV2/9-hSyn-gACh4h	Provided by Yulong Li	BrainVTA: PT-6307
Experimental models: Organisms/strains		
Long-Evans Rat	Charles River	RRID: RGD_2308852
Software and algorithms		
MATLAB 2023b	Mathworks	RRID: SCR_001622
GraphPad Prism 10.3.1	GraphPad Software	RRID: SCR_002798
ImageJ 1.54f - Fiji	Schindelin et al. ⁴⁵	RRID: SCR_002285
Bonsai 2.8	Lopes et al. ⁴⁶	RRID: SCR_021512
Custom MATLAB and Python code	This paper	Zenodo: https://doi.org/10.5281/zenodo.14729705
Other		
FP3002 photometry system	Neurophotometrics	FP3002

EXPERIMENTAL MODEL AND SUBJECT DETAILS

Experiments were performed on a total of 10 male Long-Evans rats (>3 months of age at the start of the experiment, Charles River Laboratories) housed on a 12 hr light/dark cycle at 25 °C. Rats were water restricted (10 minutes/day) for the duration of the experiments and were tested at the NIDA-IRP in accordance with NIH guidelines determined by the Animal Care and Use Committee, which approved all procedures. Rats were group housed until the execution of surgeries, after which they were single housed for the duration of the experiment. All rats had *ad libitum* access to rat chow in their home cages for the duration of the experiments. Behavior was performed during the light phase of the light/dark schedule. The lack of female rats, due to logistical issues and the fact that males performed better with the head implants, is a potential limitation of this study.

METHOD DETAILS

Surgical procedures

Rats were anesthetized with 1-2% isoflurane and prepared for aseptic surgery. They received unilateral infusions of AAV2/9-hSyn-rDA3m and AAV2/9-hSyn-gACh4h into the NAcc (AP +1.7 mm from bregma, ML + or -1.7 mm from bregma, and DV -6.3 and -6.2 mm from the brain surface, i.e., they received two infusions in the same AP and ML coordinates, but 0.1 mm from each other in DV, within the same track). Viruses were mixed in a small tube and a total 0.7 μL of this mixture was delivered in each site at 0.1 μL/min via an infusion pump. Optic fiber cannulas (200 μm diameter; Neurophotometrics, CA) were implanted in each site in the location of the second (most dorsal) viral infusion. All viruses were obtained from BrainVTA, and the titer for both viruses was ≥ 2.00E+12vg/ml, used as provided by the vendor. Exposed fiber ferrules and a protective black 3D-printed headcap were secured to the skull with dental cement. After surgery, rats were given Cephalexin (15 mg/kg po qd) for two weeks to prevent any infection.

Dual color fiber photometry

Fluorescent dopamine and acetylcholine signals were recorded using dual-color fiber photometry. General methods were similar to what was described previously.¹ In brief, custom fiber optic patch cables (200 μm diameter, 0.37 NA, Doric Lenses, Canada) were attached to the optic fiber ferrules on the rats with brass sleeves (Thorlabs, NJ). Fibers were shielded and secured with a custom 3D-printed headcap-swivel shielding. Recordings were conducted using an FP3002 system (Neurophotometrics, CA), by providing 560

(active green signal), 470 (active green signal) and 415 nm (isosbestic reference) excitation light through the patch cord in interleaved LED pulses at 150 Hz (50 Hz acquisition rate for each channel). The light was reflected through a dichroic mirror and onto a 20× Olympus objective. Excitation power was measured at ~70-90 μW at the tip of the patch cord. Emitted fluorescent light was captured via a high quantum efficiency sCMOS camera (Neurophotometrics, CA). Signals were acquired and synchronized with behavioral events using Bonsai.⁴⁶ Specifically, both photometry signals and strobe signals indicating each behavioral event (light on, nose poke and unpoke, reward delivery, reward well entry and exit) were relayed to Bonsai via USB connections. Bonsai recorded the timestamps of the sCMOS camera frames and the behavior event strobes within the same PC clock, and thus allowed for synchronization of the two types of events.

Histological procedures

After completion of the experiment, rats were perfused with chilled phosphate buffer saline (PBS) followed by 4% paraformaldehyde in PBS. The brains were post-fixed in 4% PFA for at least 24 hours then immersed in 30% sucrose in PBS until they sank, and then frozen. The brains were sliced at 50 μm, stained with DAPI (Vectashield-DAPI, Vector Lab, Burlingame, CA), and processed for immunohistochemical detection of green and red fluorescent proteins (Figures 1A, S4B, and S4C). For immunohistochemistry, the brain slices were first washed with PBS (5x10 mins), blocked in 4% BSA with 0.3% Triton X-100 in PBS, and then incubated with anti-GFP (1/1000, RT, overnight, chicken anti-GFP, ab13970, Abcam USA, Waltham, MA) and anti-RFP antibodies (1/1000, RT, overnight, rabbit anti-DsRed, 632496, Takara Bio USA, Madison, WI), followed by Alexa-488 (1/100, RT, 2h, Donkey anti-chicken Alexa Fluor 488, ab2340375, Abcam, Waltham, MA) and Alexa-594 (1/100, RT, 2h, Donkey anti-rabbit Alexa Fluor 594, ab2340621, Abcam, Waltham, MA) secondary antibodies. We want to call attention that the chicken anti-GFP antibody used here was the most successful at detecting the gACh4.0h sensor. We tested several alternatives (data not shown), made in different species and from different vendors, and highly recommend the use of this antibody for this sensor. Fluorescent microscopy images of the slides were acquired with an Olympus VS120 microscope (Figure 1A) for fiber placement confirmation and a Zeiss LSM880 Airyscan/CY7.5 confocal microscope (Figure S2) for detailed quantification of expression overlap.

QUANTIFICATION AND STATISTICAL ANALYSIS

Signal analysis

Photometry signals were processed using custom scripts in Python and MATLAB (MathWorks, MA). We filtered raw fluorescence signals from each of the 470 nm (active), 560 nm (active), and 415 nm (reference) channels with a causal median filter and a second-order Butterworth low-pass filter with a cutoff frequency of 5 Hz. Next, each channel data was fitted with a double exponential function, and the fitted data was subtracted from the original signal which removed the exponential decay artifact caused by photobleaching. The resulting signal was z-scored for each trial, using the three seconds before each trial onset, i.e., in the preceding inter-trial interval (ITI) period, as a baseline. The same trial-based baseline was used for z-scoring signals aligned to all events. For the supplemental reference control analysis, the reference (415 nm) channel data was fitted to each active signal using second-order polynomial regressions, and the fitted data was subsequently subtracted from the active channel and divided by the exponential fit of the active channel.

Cross- and autocorrelations were conducted on one second windows using MATLAB's *x-corr* function. Periods for the execution of the analyses started at ~2 seconds before light onset (baseline), immediately after light onset (light on), one second preceding nose poke (ramp), immediately after nose poke (poke), 0.5 second before unpoke (unpoke), and immediately after reward delivery (reward). The 95% confidence interval was derived by repeatedly calculating Pearson's *r* after one of the photometry signals was shifted in time (aligned to the light onset and spanning the whole trial) and then extracting the 2.5th and 97.5th percentiles across the correlation window for each bin, similar to what has been used previously.¹⁹ To address whether the dynamics of acetylcholine and dopamine to each event derive from the other signaling, we isolated the component of one signal that could not be predicted by the other signal by regressing the data of one neurotransmitter to predict the other and subtracting this predicted component from the original signal. Slopes of signals were analyzed using MATLAB's *polyfit* function.

To address whether the dynamics of dopamine and acetylcholine influence each other, we isolated the component of one signal that could not be predicted by the other signal by regressing the data of one neurotransmitter to predict the other and subtracting this predicted component from the original signal. The regression was done by using the data, *x*, in the past 2 seconds to predict the current response of the other neurotransmitter, *y*, using a double exponential kernel:

$$k = a_1 \exp\left(-\frac{t-t_1}{s_1}\right) + a_2 \exp\left(-\frac{t-t_2}{s_2}\right) \quad (\text{Equation 1})$$

$$y = (k * x)(t) \quad (\text{Equation 2})$$

where $(k * x)(t)$ indicates the linear convolution between data *x* and kernel *k*. Parameters *a*₁ and *a*₂ control the amplitude, *t*₁ and *t*₂ represent time shifts for each phase, and time constants *s*₁ and *s*₂ govern the sharpness.

We optimized these parameters for each session by minimizing mean squared error. With the optimized parameters, we were able to predict one signal based on the historical data of the other through convolution with the fitted kernel. Subsequently, this predicted component was removed from the original signal and tested to see if the response to each event was changed afterward.

Generalized linear model analysis

We performed generalized linear model (GLM) regressions following previous examples in the literature^{28,29} to measure event-related effects on the photometry signal dynamics. We also used GLMs to isolate the effects of movement by comparing responses associated with similar movements that occurred within trials and during the ITI, i.e., inside and outside of the task's trial contexts. For this, we first applied a high-pass filter (second-order Butterworth filter with a cutoff frequency of 0.001 Hz) to remove slow drifts and ensure robust results, as done previously.²⁹ The response to each event was considered as the linear convolution of the time course of the task variables with its corresponding kernel using 0.2s bins.

$$\text{signal} = b + \sum_i [k_i f(x_i)(t)] + \text{error}$$

where b is a constant, x_i is the i th variable, k_i is the corresponding kernel, and $k_i f(x_i)(t)$ indicates the linear convolution between $f(x_i)$ and k_i . Nine events: light onset, nose port poke in trials, nose port pokes in the ITIs, unpoke, early unpoke, reward onset, and reward port unpoke were included in the regression. For external presentation events (light onset, reward onset), we applied a causal kernel spanning 0 to 2 seconds, while for motor events (all other events), we used a non-causal kernel spanning -1 to 2 seconds. This linear regression model successfully captured a significant amount of variance in the signals ($r^2 = 0.15 \pm 0.02$ for dopamine, $r^2 = 0.10 \pm 0.03$ for acetylcholine).

Behavioral apparatus and instrumental nose poke task

Rats were trained and tested at least four weeks after the surgeries. Water was restricted to ~10 min free access every day for at least two days prior to training initiation. During training, they received their water ration after their daily session. All behavior experiments were conducted in custom-built aluminum chambers approximately 18' on each side with sloping walls narrowing to an area of 12' x 12' at the bottom. A central nose poke port consisting of a small hemicylinder accessible was located about 2 cm above a fluid well, and higher up on the same wall were mounted two lights. Trial availability was signaled by the illumination of the panel lights. When these lights were on, if rats performed a 500 ms nose poke into the odor port and then made a response into the fluid well and held for 500 ms, they would receive a ~0.05 mL drop of water. Rats were trained until they could reliably perform over 75 trials in a one-hour period. In a subset of rats (N=6) we also analyzed responses to nose poke performed during the ITIs.

Expression overlap analysis

To quantify if the two sensors, gACh4h and rDA3m were expressed in the same cells, we measured the overlap of the signal expression in both the green and red channels in confocal images captured at 20x. Quantification was performed using FIJI⁴⁵ according to these steps: we first converted RGB images from each channel to 16 bit, applied a Gaussian blur filter with a 3 pixel radius, and performed an IsoData threshold, with the resulting image used to create an ROI selection. We then measured the area fraction of overlap between the ROIs. Representations of these ROI overlaps were included in [Figures 1C](#) and [S2](#), along with the original RGB confocal images from the histological sections.

Statistical analysis

Statistical analyses were performed in MATLAB and GraphPad Prism. Differences between cross-correlation parameters were tested with repeated measures ANOVA and Tukey's post-hoc test. Significant differences between the signals and shuffled controls were conducted using permutation tests,²⁷ with a consecutive threshold of fifteen and ten thousand permutations. Differences between GLM regression coefficients were tested using single-sample t-tests for each 0.2s bin. In cases where two variables were compared, significant differences were tested using paired t tests or Wilcoxon tests, depending on whether the variables were normally distributed or not, respectively, according to the Shapiro-Wilk normality test. Statistical significance was set at $P < 0.05$ for all tests.